Journal of Modern Optics
Vol. 54, Nos. 13–15, 10 Sep–15 Oct 2007, 1939–1958

A short perspective on long crystals: broadband wave mixing and its application to ultrafast quantum optics

P. WASYLCZYK*†‡, A. B. U'REN§, P. J. MOSLEY†, J. LUNDEEN†, M. P. A. BRANDERHORST†, S.-P. GORZA¶, A. MONMAYRANT†, A. RADUNSKY†‖ and I. A. WALMSLEY†

†Clarendon Laboratory, University of Oxford, Parks Road, Oxford OX1 3PU, UK
‡Institute of Experimental Physics,Warsaw University, ul. Hoza 69, 00-681 Warsaw, Poland
§División de Física Aplicada, Centro de Investigación Científica y de Educación Superior de Ensenada, A.P. 360, Ensenada, Baja, California 22800 México
¶Service d'optique et acoustique, Université libre de Bruxelles 50, Av. F.D. Roosevelt, CP-194/5, B-1050 Brussels, Belgium
‖Institute of Optics, University of Rochester, Rochester, New York 14627, USA

(*Received 16 March 2007; in final form 2 May 2007*)

We present an overview of recently developed ideas in ultrafast nonlinear optics, and describe three applications where these ideas have had an impact. A closer look at three wave mixing of broadband electromagnetic fields in birefringent nonlinear crystals shows that not only phase matching, but also group velocity matching is important for understanding the process of up- and down-conversion with ultrashort laser pulses. In fact the higher-order dispersion of nonlinear crystalline materials provides an underused degree of freedom that allows tailoring the interaction so that it is suitable for a number of different applications. We analyse the processes of parametric downconversion for the production of pure single photon states, and upconversion for ultrashort pulse characterization and for quantum state and process tomography in molecules.

1. Introduction

Phase matching is a well-established concept, developed by Bloembergen [1] over 45 years ago in the context of nonlinear interactions of coherent optical electromagnetic fields. It would seem that an idea so central to the field for so long would have been completely explored, and there would be little or nothing new to say. But it is possible to teach an old dog new tricks, and recent developments in ultrafast optics

* Corresponding author. Email: pwasylcz@fuw.edu.pl

Journal of Modern Optics
ISSN 0950–0340 print/ISSN 1362–3044 online © 2007 Taylor & Francis
http://www.tandf.co.uk/journals
DOI: 10.1080/09500340701432599

have shown that the dispersion of nonlinear optical materials used in wave mixing provides a previously underestimated degree of freedom that enables a number of novel configurations well suited to certain applications.

Phase matching has been extensively exploited in all types of frequency conversion schemes ever since the first explicit notion appeared in 1962 [2, 3]. The principles of phase matching can be understood by means of two complementary pictures. On the one hand, one may consider an external electric field interacting with bound electrons in a transparent material—the polarization induced by the driving field must have a wavelength in the material that is equal to the wavelength of the electromagnetic wave generated by the anharmonic motion of the driven electrons if their contributions are to interfere constructively to generate a large output field at the new frequency. On the other hand, one may think in terms of the scattering of particles of light—photons—for which the energy and momentum of the input and output particles must be conserved. As before, the two quantities are linked by the dispersive properties of the medium.

Quasi phase matching (QPM) [1, 4] provides an ingenious means by which the phase velocities of the polarization and the generated wave can be made equal, in this case by periodically changing the sign of the nonlinear response just at the point where the polarization and the generated field are shifted in phase by π radians, thus ensuring that power always flows into the generated wave. The stunning progress in the past decade in preparing microstructures in nonlinear optical media shows how powerful this method can be in a wide variety of applications—enabling wave mixing for almost any wavelength and for any bandwidth. What we are interested in here however, goes beyond matching phase velocities, toward managing the group velocity and group velocity dispersion in order to tailor the nonlinear responses of the medium to a specific application.

With the advent of ultrashort laser pulse technology, it was realized that a quasi-monochromatic wave approach is no longer appropriate and a new challenge emerged: to understand phase matching in the case of coherent, broadband fields interacting in nonlinear optical crystals [5–9]. At first glance, it may seem that broadband frequency conversion is restricted by the phase matching characteristics of nonlinear crystals: generating the second harmonic of a femtosecond infrared laser pulse while preserving the pulse duration (i.e. without narrowing the spectrum) requires crystal lengths not exceeding a fraction of a millimetre, thus preventing high conversion efficiency. Deeper understanding of the process when ultrashort laser pulses are involved has lead to a new picture taking into account the phase mismatch for the range of frequencies involved in the process [10]. Indeed, the phrase 'second harmonic generation' is no longer appropriate—the process is more correctly referred to as sum frequency generation, since in many cases every frequency in the pulse may interact with any other frequency. The key elements in this approach are the group velocities of the interacting pulses, and controlling these is generally much harder than controlling the phase velocities by means of QPM. Nonetheless, it is both possible to find materials in which the dispersion is favourable and to imagine optical microstructures that are engineered to allow group velocity matching.

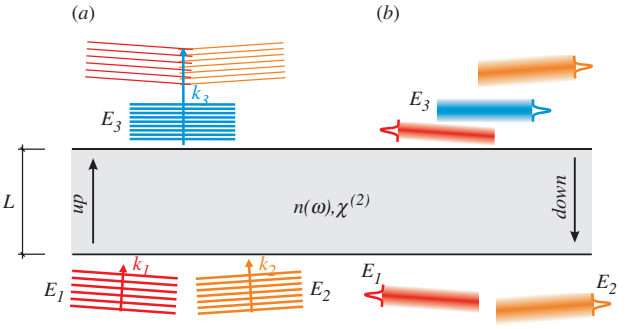

Figure 1. (*a*) Phase and (*b*) group velocity matching in a generic three-wave mixing process: three electric fields interact in a nonlinear medium of thickness L via second-order nonlinearity characterized by $\chi^{(2)}$. Dispersive properties of the medium are described by the frequency-dependent refractive index $n(\omega)$. Depending on the directions of the process we have either up- or down-conversion. In the spontaneous downconversion (SPDC) only pump (E_3) is present at the beginning. (The colour version of this figure is included in the online version of the journal.)

Thus, what initially might seem to be a limiting factor has actually proved to provide a new, valuable degree of freedom and triggered a whole range of new applications. Among them, we describe three recent techniques from quantum optics: single-photon generation in pure spectral state, characterization of quantum states of molecular vibrations via highly sensitive time-and-frequency resolved spectroscopy, and a wide class of ultrashort laser pulse characterization techniques based on spectral interferometry.

2. Phase matching of broadband fields

In this paper, we will focus on three wave mixing processes in nonlinear birefringent crystals. In such a process, three electric fields interact through the nonlinear coefficient of the material $\chi^{(2)}$. In the case of two input fields E_1, E_2 and one output field E_3, the process is known as upconversion whereas in the opposite case as downconversion, as depicted schematically in figure 1. Here, we will limit our analysis to sum frequency generation, where the frequencies of the respective fields obey $\omega_{1,2} < \omega_3$. In an upconversion process, the input fields are called the fundamental beams (or pulses), while in the downconversion, the input field of higher frequency ω_3 is referred to as the pump, and the resulting ones as signal and idler (with an arbitrary assignment).

Whatever form the interacting fields may have, in the collinear interaction of plane waves, we can write the energy and momentum conservation in the form [7]

$$\tilde{E}_3(\omega_3) \sim \int\int \mathrm{d}\omega_1 \mathrm{d}\omega_2 \delta(\omega_1 + \omega_2 - \omega_3)\tilde{E}_1(\omega_1)\tilde{E}_2(\omega_2)\Phi(\omega_1, \omega_2), \tag{1}$$

where the fields $E_{1,2,3}$ are represented in the spectral domain by their respective Fourier transforms $\tilde{E}$ and $\Phi(\omega_1, \omega_2)$ is the phase matching function (PMF)—the protagonist of this paper. For a nonlinear crystal of length L the phase matching function is given by

$$\Phi(\omega_1, \omega_2) = \frac{\sin\left((1/2)L\Delta k\right)}{(1/2)L\Delta k} \exp\left(\mathrm{i}(1/2)L\Delta k\right), \tag{2}$$

the wavevector mismatch in the collinear case being $\Delta k = k_1(\omega_1) + k_2(\omega_2) - k_3(\omega_3)$ where $k(\omega)$ is the wavevector length.

The Dirac delta in equation (1) results from the energy conservation while the phase matching function is a consequence of momentum conservation within the uncertainty defined by the interaction length—the smaller the crystal length L, the larger the deviation from exact momentum conservation $k_1(\omega_1) + k_2(\omega_2) - k_3(\omega_3) = 0$ is allowed in the frequency conversion process.

Two types of phase matching in a birefringent (negative) crystal are most commonly used: type I where E_1 and E_2 propagate in the crystal as ordinary rays, while E_3 is extraordinary and type II, where E_1 and E_3 are extraordinary, and E_2—ordinary.

The respective wavevector mismatches in the two cases read

$$\Delta k_{\mathrm{oo}\leftrightarrow\mathrm{e}} = \frac{2\pi n_{\mathrm{o}}(\lambda_1)}{\lambda_1} + \frac{2\pi n_{\mathrm{o}}(\lambda_2)}{\lambda_2} - \frac{2\pi n_{\mathrm{e}}(\lambda_3)}{\lambda_3}, \tag{3}$$

$$\Delta k_{\mathrm{oe}\leftrightarrow\mathrm{e}} = \frac{2\pi n_{\mathrm{e}}(\lambda_1)}{\lambda_1} + \frac{2\pi n_{\mathrm{o}}(\lambda_2)}{\lambda_2} - \frac{2\pi n_{\mathrm{e}}(\lambda_3)}{\lambda_3}, \tag{4}$$

where n is the refractive index of the medium and, as throughout the paper, the 'o' and 'e' subscripts indicate ordinary and extraordinary rays in the crystal. Generally, one can plot a map of the magnitude of the PMF as a function of ω_1 and ω_2 for a particular crystal length and orientation. For a common KDP (potassium dihydrogen phosphate) negative, uniaxial crystal such maps for type I and type II collinear three wave mixing are presented in figure 2 for $\omega_{1,2,3}$ spanning the KDP transparency range between 0.24–1.5 μm. In both cases the crystal angle is set for perfect degenerate phase matching at 830 nm.

To explore the broadband phase matching in both types of interactions, we will examine the phase matching function map in the vicinity of $\Delta k = 0$ around the degenerate fundamental wavelength—figure 3. The degenerate case is of particular practical importance: in up-conversion it means that the electric field can interact with itself or with its time-delayed replica, while in down-conversion it allows one to generate photon pairs in which both particles have spectra centred on the same central frequency.

The wavevector length can be expanded into a Taylor series in the vicinity of ω_0

$$k(\omega) = k(\omega_0) + \frac{\partial k(\omega)}{\partial \omega}(\omega - \omega_0) + \frac{1}{2}\frac{\partial^2 k(\omega)}{\partial \omega^2}(\omega - \omega_0)^2 + \cdots. \tag{5}$$

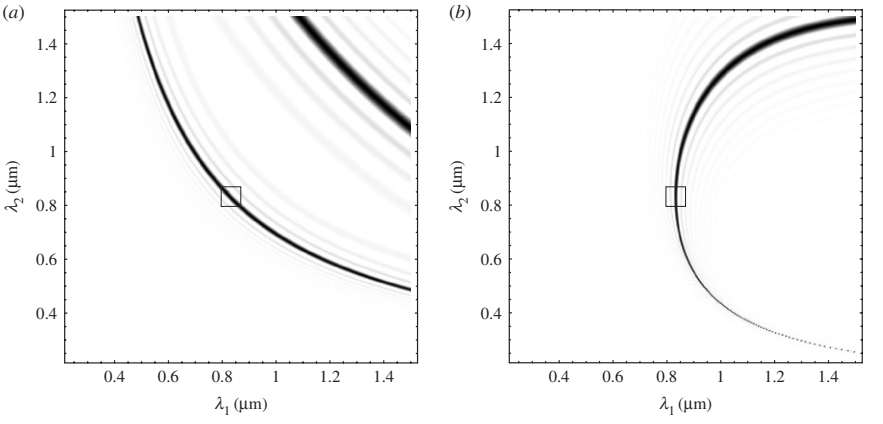

Figure 2. Magnitude of the phase matching function $\Phi(\lambda_1, \lambda_2)$ calculated within the transparency range of KDP for (*a*) type I and (*b*) type II interactions. The phase matching angle was set for perfect phase matching at degeneracy at 830 nm, the crystal thickness is 2 mm. The squares indicate the region enlarged in figure 3. Darker regions correspond to higher value, white being 0 and black 1.

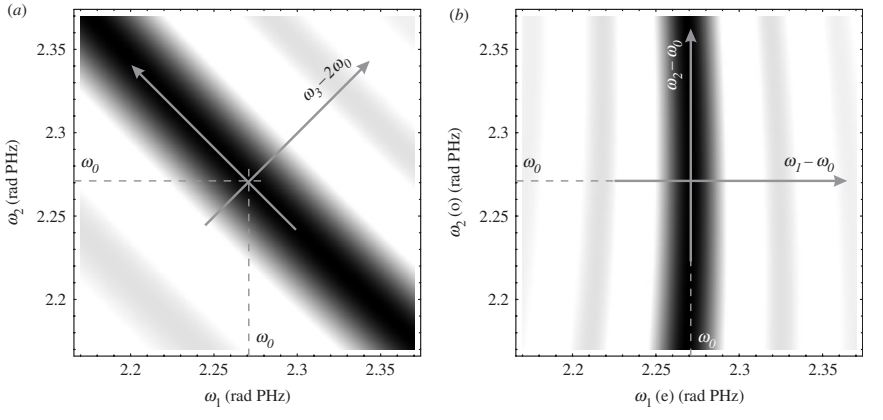

Figure 3. Magnitude of the phase matching function $\Phi(\omega_1, \omega_2)$ in the vicinity of the $\Delta k = 0$ chosen to be at $\omega_1 = \omega_2 = \omega_0 = 2.271$ PHz for 2 mm KDP crystal in the case of (*a*) type I and (*b*) type II interaction. Darker regions correspond to higher value, white being 0 and black 1.

The first derivative on the right-hand side $\beta(\omega) = \partial k(\omega)/\partial\omega$ is the inverse of the group velocity, the second one $\partial^2 k(\omega)/\partial\omega^2$ is the group velocity dispersion and the higher orders of dispersion are neglected.

In particular, for the type I process, expanding the wavevector mismatch (3) around $\Delta k(\omega_0, \omega_0) = 0$ and keeping only the first-order terms, gives

$$k_o(\omega_1) = k_o(\omega_0) + (\omega_1 - \omega_0)\beta_o(\omega_0), \tag{6}$$

$$k_o(\omega_2) = k_o(\omega_0) + (\omega_2 - \omega_0)\beta_o(\omega_0), \tag{7}$$

$$k_e(\omega_1 + \omega_2) = k_e(2\omega_0) + (\omega_1 + \omega_2 - 2\omega_0)\beta_e(2\omega_0) \tag{8}$$

and the wavevector mismatch now reads

$$\Delta k_{\mathrm{oo}\leftrightarrow\mathrm{e}} = (\omega_1 + \omega_2 - 2\omega_0)(\beta_{\mathrm{o}}(\omega_0) - \beta_{\mathrm{e}}(2\omega_0)). \tag{9}$$

Keeping in mind the form of the $\sin((1/2)L\Delta k)/(1/2)L\Delta k$ function that governs the behaviour of the phase matching magnitude we notice that it is the group velocity difference that determines the shape of $\Phi(\omega_1, \omega_2)$. The width of the $\Psi(\omega_1 = \omega_2)$ cross-section, corresponding to the ω_3 bandwidth involved in the process, increases with decreasing difference between the group velocities of the fundamental beam and the sum-frequency beam (or the difference between group velocities of the pump and spectrally degenerate downconverted beams in down-conversion).

Applying the same expansion for the type II process, the wavevector mismatch is

$$\Delta k_{\mathrm{oe}\leftrightarrow\mathrm{e}} = (\omega_1 - \omega_0)(\beta_{\mathrm{e}}(\omega_0) - \beta_{\mathrm{e}}(2\omega_0)) + (\omega_2 - \omega_0)(\beta_{\mathrm{o}}(\omega_0) - \beta_{\mathrm{e}}(2\omega_0)). \tag{10}$$

Now one can see that if the two conditions are fulfilled, namely: (1) the group velocity of the ordinary fundamental ray matches the group velocity of the extraordinary sum frequency ray, and (2) the group velocity of the extraordinary fundamental ray differs from the group velocity of the sum frequency ray, the asymmetric phase matching magnitude results in a broad acceptance bandwidth for the ordinary beam and a narrow acceptance bandwidth for the extraordinary one as plotted in figure 3(*b*).

Consequently, in the up-conversion process, by selecting the appropriate type of interaction, crystal orientation and thickness, one can determine the range of frequencies taking part in the wave mixing process for both fundamental and upconverted beams. In down-conversion, the joint spectrum of the photon pair can be engineered in the same way.

The higher order terms that we have neglected in the Taylor series expansion account for group velocity dispersion (GVD) and higher orders of dispersion. They lead to distortion of the phase matching function from the simple 'linear' form and become important in the case of extremely broadband fields [11].

3. Engineering spectrally pure single-photon states

The generation of two-photon states characterized by a factorable joint amplitude is crucial for a number of quantum information technologies, including pure-state heralded single-photon production. In this section, we show how one can create these factorable states through the process of spontaneous parametric downconversion (SPDC) in a nonlinear $\chi^{(2)}$ crystal by matching the group velocities of the constituent fields. In the process of SPDC, pump photons split into pairs of daughter photons; one of these photons can then be used to herald the arrival of its twin. For an initial two photon state that has correlations between the pairs of photons in any degree of freedom, as is the case with most SPDC sources, detecting one photon, as a herald traces over its degrees of freedom, leaves the remaining single-photon state mixed.

Pure single-photon generation is a necessary technology for experiments involving the concatenation of multiple single-photon sources into quantum networks, including implementations of teleportation [12, 13], entanglement swapping [14] as well as of logic gates based on quantum computation with linear optics [15]. Furthermore, only pure single-photon states can be in Fourier-transform limited, ultrashort wavepackets, which are of potential importance for quantum communication protocols [16]. Considering the higher-order terms produced in SPDC, the signal and idler modes are created in an entangled squeezed state. This too will need to be in a factorable state for the purpose of quantum information processing [17, 18]. By producing factorable states at the source, we avoid creating them through spectral and/or spatial filtering which has the drawback of an accompanying drastic reduction of source brightness and bandwidth.

In this analysis we restrict attention to the spectral degree of freedom; we assume that the signal and idler modes are filtered spatially such that a single direction of propagation for each of the two photons reaches the detection apparatus. The joint spectral state of the photon pairs produced in SPDC is closely related to the acceptance bandwidths associated with up-conversion, and is given by

$$|\psi\rangle \propto \int\int \mathrm{d}\omega_\mathrm{s}\mathrm{d}\omega_\mathrm{i}\, f(\omega_\mathrm{s},\omega_\mathrm{i})a^\dagger(\omega_\mathrm{s})a^\dagger(\omega_\mathrm{i})|vac\rangle, \tag{11}$$

$$f(\omega_\mathrm{s},\omega_\mathrm{i}) = \Phi(\omega_\mathrm{s},\omega_\mathrm{i})\ \exp(-(\omega_\mathrm{s}+\omega_\mathrm{i}-\omega_{\mathrm{p}0})^2/\sigma^2), \tag{12}$$

where the subscripts 's', 'i' and 'p' denote signal, idler and pump, respectively, $\Phi(\omega_\mathrm{s},\omega_\mathrm{i})$ is the phase matching function given in equation (1) and the exponential results from the Gaussian spectrum of the pump with a width σ and centre frequency $\omega_{\mathrm{p}0}$—see figure 4. Through $\Phi(\omega_\mathrm{s},\omega_\mathrm{i})$ and hence, Δk, the spectral structure of the photon pairs is determined in the lowest order by the group velocity mismatch amongst the three photons, as discussed in the previous section. This leads to the possibility of obtaining factorable states (i.e. $f(\omega_\mathrm{s},\omega_\mathrm{i}) = g(\omega_\mathrm{s})h(\omega_\mathrm{i})$) by engineering the entanglement properties at the source through group velocity matching (GVM) conditions.

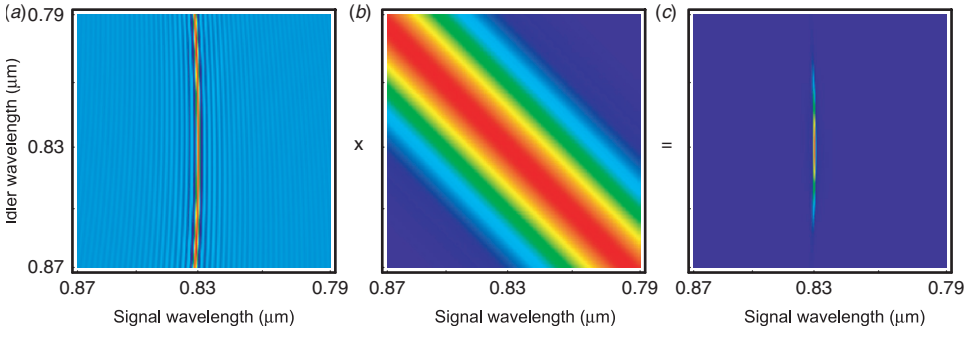

Figure 4. Construction of a factorable joint spectrum. Square of the product of the phase matching function for a 20 mm KDP crystal set for type II at 830 nm (*a*) and the broadband pump function (*b*) gives the joint spectral intensity of the two photon state (*c*). (The colour version of this figure is included in the online version of the journal.)

Examining figure 4 leads to the conclusion that factorable states can be obtained only when the angle subtended by the contours of $\Phi(\omega_s, \omega_i)$ and those of the pump function is greater than or equal to 45°. This occurs for group velocities obeying $\beta_s \leq \beta_p \leq \beta_i$ or $\beta_i \leq \beta_p \leq \beta_s$ [19]. Symmetric states, with the same bandwidth for each of the two photons, can be created when $2\beta_p = \beta_s + \beta_i$, whereas highly elongated states, where one of the photons is broadband while its conjugate is essentially monochromatic, are created when $\beta_p = \beta_s$ or $\beta_p = \beta_i$. Between these two extrema, symmetric and asymmetric, the general group velocity conditions above lead to factorable states with a varying degree of spectral elongation. Apart from the requirement on the group velocities, an important additional requirement for factorizability is that the pump bandwidth be matched to the phase matching bandwidth (which can be varied through the crystal length).

Here we concentrate on asymmetric factorable states. These are easier to produce and detect for two reasons. First, they exhibit the important property that for a sufficiently thick crystal together with a sufficiently broadband pump, the crystal length and pump bandwidth become decoupled from each other, a significant added flexibility for experimental implementations. Second, for a given $\chi^{(2)}$ material, if λ_{sym} represents the SPDC wavelength yielding symmetric GVM, $\beta_p = \beta_s$ is fulfilled at λ_{ver} and $\beta_p = \beta_s$ is fulfilled at λ_{hor}, then either $\lambda_{ver} < \lambda_{sym} < \lambda_{hor}$ or $\lambda_{hor} < \lambda_{sym} < \lambda_{ver}$. While for typical materials, λ_{sym} lies in the infrared where single photon detection technology is not well developed, either λ_{ver} or λ_{hor} can occur within the detection range of silicon avalanche photodiode detectors. Specifically, looking at figure 4(*a*), $\Phi(\omega_s, \omega_i)$ is vertical at 830 nm for a type II collinear process in KDP and itself contains no correlations between ω_s and ω_i. Therefore, if we use a broadband pump centred at 830 nm (figure 4 (*b*)), the joint spectrum $f(\omega_s, \omega_i)$ of the resulting two-photon state will be factorable as in figure 4(*c*). This wavelength region is compatible with well-established laser technology (femtosecond Ti:sapphire) *and* single photon detection technology.

The asymmetric spectral structure present in factorable, highly-elongated photon pairs leads to a number of consequences: it has been shown that while symmetric and highly elongated factorable photon pairs both result in Fourier-transform limited photon pairs, it is only for the latter that heralded single photon wavepackets can attain their shortest possible duration, which corresponds to the pump pulse duration [16]. Also, since one of the two photons is almost monochromatic the state is insensitive to the temporal broadening effects due to dispersion in the crystal itself or in other optical elements. Indeed, it has been shown that in the long-crystal limit, while the quadratic spectral phase factor due to dispersion in the crystal leads to temporal broadening of each individual photon in the pair, the mixed phase term, which would introduce temporal correlations, is suppressed [20].

Experimentally generating a factorable two-photon state requires stringent control over the parameters of the downconverted state. The most critical aspect is the exact angle of propagation of the pump relative to the optic axis of the PDC crystal. As shown in figure 5, the e-ray wavelength is highly dependent on this angle; for phase matching near 830 nm, a 1° rotation about an axis perpendicular to the plane of the optic axis and pump *k*-vector changes the e-ray downconverted wavelength by approximately 10 nm. Therefore, in order to be able to interfere the

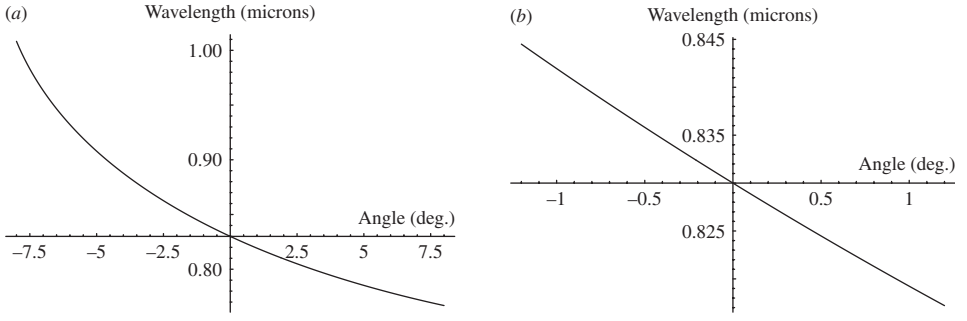

Figure 5. Plots showing the change in degenerate, collinear phase matched wavelength as a function of the phase-matching angle, plotted as the difference in degrees from the phase matching angle for degenerate, collinear PDC at 830 nm. Part (*b*) shows magnified central part of (*a*).

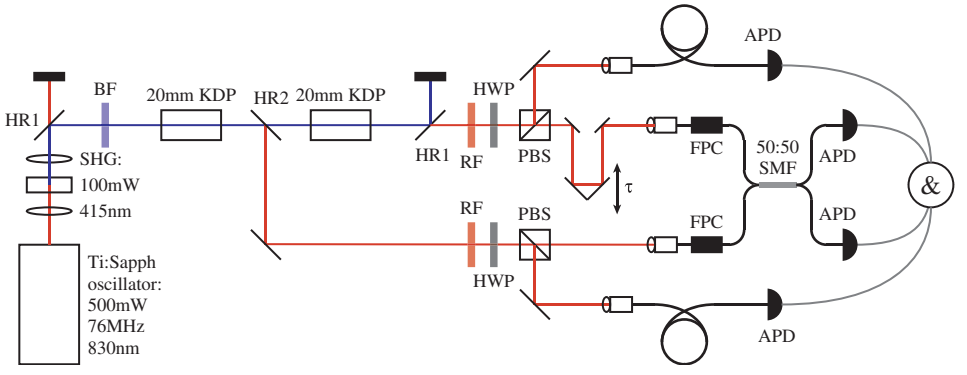

Figure 6. Experimental apparatus for measurement of the HOMI dip from two independent SPDC sources. HR1—dielectric mirror HR@415 nm, HT@830 nm, BF—blue glass filter, HR2—dielectric mirror HR@830 nm, HT@415 nm, RF—red glass filters, HWP—half wave plates, APD—avalanche photodiodes, PBS—polarizing beamsplitters, τ—delay line, FPC—fibre polarization controllers, 50:50 SMF—single mode fibre beamsplitter, and four-fold AND gate and counter. (The colour version of this figure is included in the online version of the journal.)

e-ray photons from multiple sources, one must match the propagation angle for all the sources used to ensure that all e-ray photons have exactly the same wavelength.

Type II SPDC allows the two daughter photons to be split at a polarizing beamsplitter, following which both photons are coupled into single mode fibres. Coupling into fibres ensures good mode-matching for the interference effects used in quantum information processing. Ideally, to match the above theory, the pump beam would simply be collimated when passing through the down-conversion crystal. However, in order to get good coupling efficiencies into the single mode fibres, the pump must be focused into the crystal. This results in additional complications in the scheme, as some unexpected correlations can emerge as a result of different *k*-vectors in the pump phase matching in different directions.

For the plane wave case, the bandwidth of the e-ray photons is solely dependent on the crystal length. However, focusing acts to broaden the e-ray spectrum due to the effective relaxation of the transverse phase matching constraint, even when the range of angles is small (i.e. the Rayleigh range is much larger than the crystal length). This can be modelled numerically by summing $f(\omega_s, \omega_i)$ over the range of input angles with a Gaussian weighting. Moreover, unlike in the above theory, we also collect a range of output angles into the single mode fibres. We similarly sum $f(\omega_s, \omega_i)$ over these output angles. This model allows us to predict the joint spectrum of e- and o-ray photons collected into the fibres.

An additional experimental complication arises from the effects of spatial chirp on the pump beam. To get a reasonable conversion efficiency from the fundamental Ti:sapphire laser frequency of 830 nm to the required pump wavelength of 415 nm by second harmonic generation, the pulses must be focused tightly into the second harmonic generation (SHG) crystal. This results in a wide spread of angles incident on the SHG crystal, and hence a strong correlation between the frequency of the second harmonic light and the angle at which it emerges. This angle is then mapped onto position by the collimating lens following the SHG crystal, and back onto angle by the lens before the PDC crystal. Each frequency component of the pump beam is then incident on the PDC crystal at a different angle and as such is subject to different phase matching conditions. This can introduce further correlations to the down-converted state, the elimination of which requires precise knowledge of the amount of spatial chirp, its direction, and the orientation of the crystals' optic axes. Once we know these parameters, however, we can incorporate the spatial chirp in the numerical model by correlating the input angle to the pump frequency in the above sum.

In order to test the purity of the heralded single photons produced we perform a Hong–Ou–Mandel type interference (HOMI) experiment on two heralded photons from different sources (figure 6). A Ti:sapphire oscillator (76 MHz, 830 nm, 20 nm FWHM, 500 mW) is frequency doubled in a 700 μm BBO crystal to produce a pump with FWHM of around 5 nm which is then lightly focused into two 20 mm KDP crystals cut for type II phase matching at 830 nm. A dichroic mirror between the two crystals splits off the down-converted light from the first and transmits the pump to the second. The remaining pump is filtered out using more dichroic filters and Schott glass filters. The o-ray photons are reflected at a pair of polarizing beamsplitters (PBSs) and coupled into single mode fibre for detection at two avalanche photodiodes (APDs) to act as heralds. The e-ray photons, having been transmitted at the PBSs then have a variable time delay set between them, and are coupled into the input ports of a single mode fibre 50:50 coupler. Fibre polarization controllers are used to ensure that the e-ray photons arriving at the coupler are in the same polarization.

Coincidence counts are monitored between the two heralding APDs and two more APDs at the outputs of the 50:50 coupler as a function of the optical time delay between the two e-ray heralded photons. If the two photons are perfectly temporally and spectrally overlapped when they arrive at the 50:50 coupler, and if they are indeed pure, perfect bunching will be observed and there will be no coincidences between all four detectors. On the other hand, even for perfect overlap, photons in

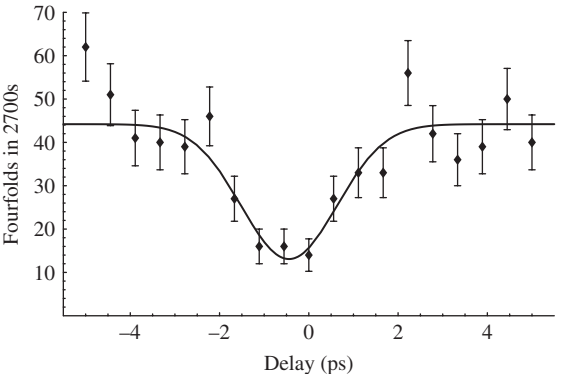

Figure 7. Measured nonclassical interference between heralded single photons from spatially separate sources.

completely mixed states will not interfere and the rate of coincidences will not decrease at zero relative delay. The visibility of the dip is equal to the purity of the photons.

Figure 7 shows experimental data of the nonclassical interference between heralded photons with a visibility of 70%, clearly breaking the nonclassical limit of 50%. The single photons produced have very low timing jitter ($\sim$1 fs) and a bandwidth of approximately 3 nm.

There are several reasons for the visibility being less than 100%. Firstly, there are effects that are not a result of mixedness in the heralded photons, including background (from erroneous singles counts and higher order down-conversion), non-perfect frequency overlap of the e-ray photons due to slightly different phase matching angles in each crystal, and non-50:50 splitting at the fibre coupler. Secondly, there are the effects of correlations in the generated two-photon state. These are a result of focusing and spatial chirp, as explained above, along with the inherent curvature in the phase matching function of KDP. We expect that our numerical model will allow us to tailor the spectral state by counterbalancing the tilt in the joint spectrum induced by these factors.

4. Tailored phase matching for spectral shearing interferometry—ultrashort laser pulse characterization

Nowadays, ultrashort optical pulses are essential tools in many research and applied fields such as spectroscopy, plasma physics, biology, medical imaging, as well as nonlinear and/or quantum optics and are beginning to enter into telecommunication technology. Many new applications require control of the pulse shape with increasing accuracy, which calls for new diagnostic devices. The ability to measure the form of the optical wave itself is indeed crucial in understanding the linear and nonlinear properties of the system through which the pulses propagate and paves the way for new experiments.

The fundamental quantity describing a pulse of light is the real electric field $\varepsilon(t)$ defined as twice the real part of the analytical signal $\varepsilon(t) = 2 \times \Re[E(t)]$. The analytical signal contains complete information about how both the intensity and the wavelength of the pulse evolve in time. As a complex quantity, $E(t)$ can be uniquely expressed in terms of amplitude and phase:

$$E(t) = |E(t)| \exp[\mathrm{i}\varphi(t) - \mathrm{i}\omega_0 t], \tag{13}$$

where the square of the envelope $|E(t)|^2$ is the time-dependent intensity, $\varphi(t)$ is the temporal phase and ω_0 is the nominal carrier frequency. It is entirely equivalent to work in the frequency domain, in which case one deals with the Fourier transform $\tilde{E}(\omega)$ of $E(t)$. The energy spectrum of the pulse, in most cases the easiest quantity to measure, is then $\tilde{I}(\omega) = |\tilde{E}(\omega)|^2$. The spectral phase $\tilde{\varphi}(\omega) = \arg(\tilde{E})$ describes the relative phase between the frequencies and the quantity $\partial\tilde{\varphi}/\partial\omega$ is usually interpreted as the group delay for the frequency ω. Knowledge of the $\tilde{I}(\omega)$ alone is not sufficient to reconstruct the pulse, because the spectral intensity, as measured in a spectrometer, contains no information about the phase of the field.

Since the duration of ultrashort optical pulses is, in many cases of interest, much shorter than the response time of any electronic detection devices, the envelope of the electric field cannot be directly measured by using photodetectors alone, but one should resort to a combination of ancillary filters to overcome this problem [21]. There are numerous, quite general strategies for characterizing the electric field of ultrashort optical pulses, each distinguished by the type of the filters used [22]. However, interferometry is perhaps the most obvious method to measure the phase of an optical field. It is based on the well known fact that the phase difference between two mutually coherent optical fields is converted into intensity modulation when the two fields are superimposed at a photodetector. An important feature of interferometric measurement is that the phase difference between the two fields can be directly extracted from the interferogram and, in addition, is quite insensitive to noise compared to other methods. Interferometry could be adapted to measure the spectral phase $\tilde{\varphi}(\omega)$, thus providing, together with the spectral amplitude measurement, a method—spectral interferometry—to completely characterize optical pulses. Spectral interferometry (SI) relies on the measurement of the spectral intensity of the pulse under study combined with a reference pulse delayed by τ (see figure 8(a)). The resulting spectral interferogram $S(\omega)$ is given by

$$S(\omega) = \tilde{I}_{\mathrm{Test}} + \tilde{I}_{\mathrm{Ref}} + 2\left(\tilde{I}_{\mathrm{Test}}\tilde{I}_{\mathrm{Ref}}\right)^{1/2}\cos[\tilde{\varphi}_{\mathrm{Test}} - \tilde{\varphi}_{\mathrm{Ref}} - \omega\tau]. \tag{14}$$

Equation (14) shows that the phase difference $\theta(\omega) = \tilde{\varphi}_{\mathrm{Test}} - \tilde{\varphi}_{\mathrm{Ref}}$ between test and reference pulses is encoded in the fringe spacing nominally equal to $2\pi/\tau$ (see figure 8(b)). τ is chosen to provide enough fringes in the spectrum to resort to standard fringe inversion techniques to extract $\theta(\omega)$. Of course this approach requires the knowledge of the spectral phase of the reference pulse and, since it must cover the same spectral bandwidth as the test pulse, characterizing the reference is exactly the problem we intend to solve.

Some time ago, an elegant solution was proposed in which the reference pulse is nothing but a replica of the test pulse, frequency shifted by a small amount Ω referred to as the frequency shear [23]. In this case the extracted phase is

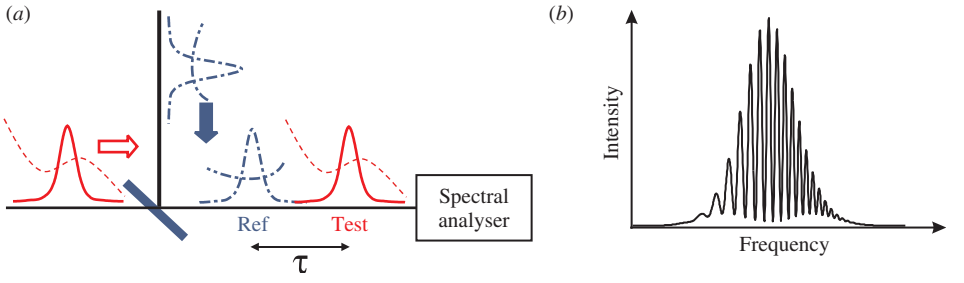

Figure 8. (*a*) Conceptual setup for spectral interferometry. (*b*) Spectral interferogram: the fringes are nominally spaced by $2\pi/\tau$. (The colour version of this figure is included in the online version of the journal.)

$\tilde{\varphi}(\omega) - \tilde{\varphi}(\omega - \Omega) - \omega\tau$. After subtracting the calibration term $-\omega\tau$, the phase $\tilde{\varphi}(\omega)$ is directly obtained by concatenation or integration of the phase difference $\theta(\omega; \Omega) = \tilde{\varphi}(\omega) - \tilde{\varphi}(\omega - \Omega)$. An implementation of this technique labelled *spectral phase interferometry for direct electric field reconstruction* or SPIDER is now routinely used to measure ultrashort pulses in the femtosecond domain. In SPIDER, the sum frequency generation (SFG) in a $\chi^{(2)}$ medium is the mechanism used to generate an adequate shear without distorting the spectral phase for pulses with broad spectra. The self-referenced interferogram is usually produced by mixing, in a nonlinear crystal, two replicas of the unknown pulse with two quasi-monochromatic waves separated in frequency by the shear. Such an implementation requires generation of the quasi-monochromatic waves and a thin nonlinear crystal characterized by a phase matching function allowing a broadband test pulse to mix with a narrowband ancilla.

Recently, we have shown that a thick nonlinear crystal, properly chosen to exhibit a nearly vertical PMF as depicted in figure 2(*b*), may be used to generate the spectral shear, eliminating the requirement for quasi-monochromatic ancillary pulses and the optical components to produce them [24, 25]. In this case, the ordinary incident pulse (o-wave) has a large acceptance bandwidth, whereas the extraordinary wave (e-wave) has a much narrower acceptance bandwidth. As we have shown above, this highly asymmetric PMF shape is the result of a group velocity match between the ordinary fundamental input and the extraordinary upconverted output and a group velocity mismatch between the extraordinary and the ordinary fundamental pulses. Because of this specific PMF, the entire bandwidth of the ordinary pulse is upconverted with a single extraordinary pulse frequency, resulting in replication of the former at the upconverted frequency. The exact narrowband component of the extraordinary pulse that upconverts with the ordinary pulse is determined by the angle of propagation relative to the crystal optic axis. Thus, the two spectrally sheared copies of the test pulse required by spectral shearing interferometry can be generated by two beams with slightly different angles of propagation as presented in figure 9(*a*).

From equation (2), one may be tempted to think that the longer the crystal, the better the replication, since the phase matching function is narrower and the width of the efficiently mixed extraordinary wave component is therefore narrower too.

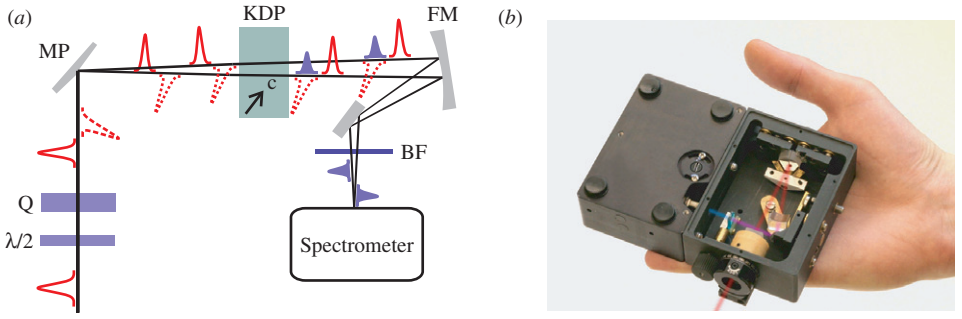

Figure 9. Setup of a long-crystal SPIDER device: $\lambda/2$—half-wave plate, Q—quartz block, MP—mirror pair, KDP—nonlinear crystal, *c*—optic axis, FM—focusing mirror, BF—blue glass filter (*a*) and practical implementation of micro-SPIDER in a compact device attached to a miniature spectrometer (*b*). (The colour version of this figure is included in the online version of the journal.)

However, this is not true, first because we deal with ultrashort pulses, and second because the extraordinary and the ordinary group velocities do not match. Indeed, if we assume that the test pulse has a compact temporal support Δt, then the maximum interaction length is $2\Delta t/\Delta k'$, where $\Delta k'$ is the group velocity mismatch between the two fundamental waves. However, such an interaction length can be achieved only if the fastest pulse is predelayed at least by Δt with respect to the slowest one before the crystal and we have shown that the predelay is essential for an undistorted up-conversion [26]. As a result, in practical implementations, the maximum time support of the pulse that can be accurately measured is determined by the predelay and the crystal length.

Figure 9(*a*) shows the SPIDER setup with a long nonlinear crystal. The linearly polarized input pulse is first split into the ordinary and the extraordinary polarizations by passing through a $\lambda/2$ waveplate and a 10 mm thick crystalline quartz plate, the e-wave being predelayed by 317 fs with respect to the o-wave. The beam is subsequently split into two beams angularly separated by approximately 0.25° by a mirror pair. The beams are sent onto a 5 mm thick KDP crystal cut for type II second harmonic generation at 830 nm (horizontal optic axis). Due to the phase matching function, the angular offset of the fundamental beams in the crystal leads to a spectral shift (shear) of around 0.8 nm between the two up-converted pulses. At the crystal output a focusing mirror recombines the beams onto the entrance slit of a compact grating spectrometer (USB2000, Ocean Optics). The delay τ between the up-converted pulses is achieved by translating one of the mirrors in the mirror pair. Practical realization of the compact SPIDER is shown in figure 9(*b*). Figure 10(*a*) displays a typical experimental interferogram measured with the long crystal device. The 1.5 ps delay results in the rapidly varying fringes. The corresponding reconstructed temporal intensity and phase of the pulse is shown in figure 10(*b*).

The unique asymmetric properties of the type II phase matching function in a long crystal can also be exploited to generate a two-dimensional interferogram from which the temporal properties of the pulse can be extracted. Indeed, by focusing the fundamental beam into the nonlinear crystal, the central wavelength of the

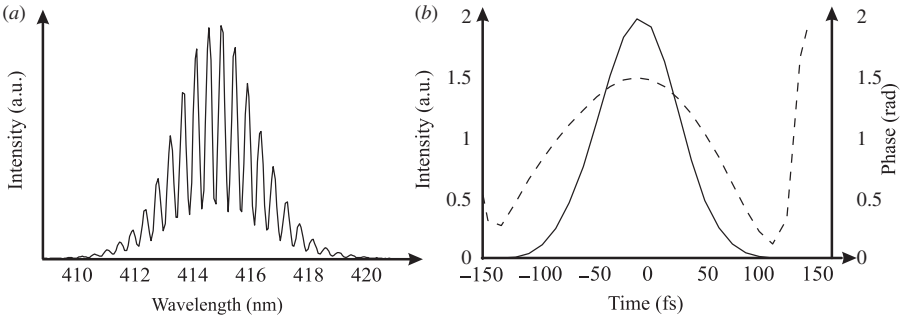

Figure 10. (*a*) Experimental SPIDER interferogram. (*b*) Reconstructed pulse temporal intensity and phase.

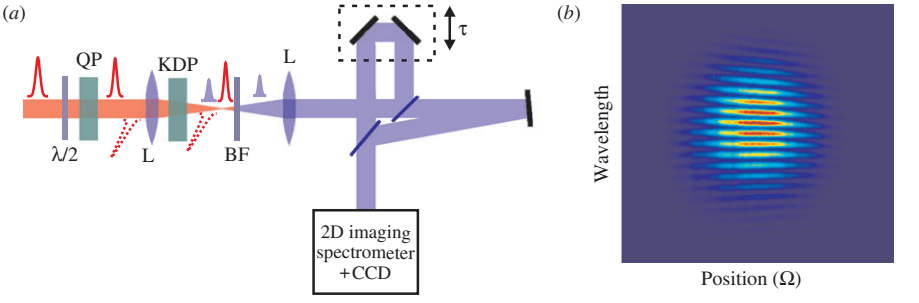

Figure 11. (*a*) Experimental setup of SPIDER using a spatially chirped beam generated by focusing the fundamental beam into the long nonlinear crystal. λ/2—half waveplate, QP—quartz plate, L—lens, KDP—nonlinear crystal, BF—blue glass filter. (*b*) 2D interferogram of a chirped pulse. (The colour version of this figure is included in the online version of the journal.)

upconverted beam is no longer uniform across the beam but changes linearly in the plane of the crystal optic axis. This feature, the spatial chirp, results from the fact that the focusing lens generates a continuous range of beam propagation directions, each selecting a different frequency component of the e-wave that up-converts with the o-wave. The recombination of this *spatially chirped* beam with its own mirror image having a reverse spatial chirp at an imaging spectrometer results in a two-dimensional interferogram as shown in figure 11. From this interferogram alone, the phase difference $\theta(\omega;\Omega)$ for a continuous range of spectral shears can be extracted. In particular, the reference phase $-\omega\tau$ does not need to be calibrated separately as in classical SPIDER. The strong redundance in the 2D interferogram also enables us to check the consistency of the reconstruction.

5. Complete tomographic measurement of weak molecular fluorescence

Apart from the interferometric techniques, there is another class of methods used in ultrashort laser pulse characterization—the spectrographic techniques. Time and

frequency filters arranged in series can be used to measure a two-dimensional map of the pulse from which the amplitude and phase of the electric field are retrieved [27]. As figure 3(*a*) indicates, using a type I nonlinear crystal with properly chosen thickness in the sum frequency generation, is equivalent to using a system consisting of a thin nonlinear crystal and a spectral filter acting on the output sum frequency wave—the system required for spectrographic measurement.

We have demonstrated that simultaneous spectral and temporal filtering of the signal in sum frequency generation in a thick type I nonlinear crystal enables us to characterize femtosecond light pulses in a simplified setup with increased sensitivity [10, 28]. The same phase matching properties of the type I process in combination with ultrashort laser pulses allow one to perform time- and frequency-resolved measurements of incoherent fields such as the molecular fluorescence, with increased signal as well as signal-to-noise ratio [29] and can be used for quantum state characterization of diatomic molecules via quantum tomography.

The Heisenberg uncertainty relations predict that conjugate variables of a single system cannot be measured independently without back-action, while the no-cloning principle states that one can not perfectly copy a quantum system in order to perform multiple measurements. A way out of this problem is to identically prepare a series of states from the same statistical ensemble, a general method referred to as quantum tomography [30, 31]. If a sufficient number of identically prepared states is available and the correct measurements are chosen, it allows a complete reconstruction of the density matrix. With the reconstructed density matrix the outcomes of all possible measurements are known as well as, in the case of unitary evolution, the past and future of the system. Because of the entanglement of a system with its environment, however, the evolution will most often be a nonunitary transformation of the density matrix. A more general framework of quantum transformations is required to understand the system evolution in such cases—quantum process tomography provides such a framework [32].

State tomography of diatomic molecular vibrational wavepackets was first implemented by Dunn *et al*. [33, 34]. A range of energy levels is excited coherently by applying a resonant broadband laser pulse to the molecular system, thus forming a wavepacket. Since the latter is not an eigenstate of the vibrational Hamiltonian in the excited electronic state, it performs a periodic motion in the molecular potential around the equilibrium internuclear separation. In the phase space of internuclear coordinate and momentum this corresponds to a rotation. During its evolution the molecule emits radiation spontaneously. Because the electronic and vibrational degrees of freedom are coupled, the internuclear separation is mapped onto fluorescence wavelength. It was realized quite early on that simultaneous time- and frequency-gated optical emission spectra could track wavepacket motion in diatomic molecules [35]. With an ideal detection system the wavelength-dependent intensity of the fluorescence is similar to the shape of the probability distribution of the position of the wavepacket. If the mapping of frequency onto internuclear separation is unique, the time-dependent spectrum is tomographically complete. The measurement procedure involved turns out to be closely related to spectrographic measurement of pulsed electric fields using time and frequency filters (compare figure 12).

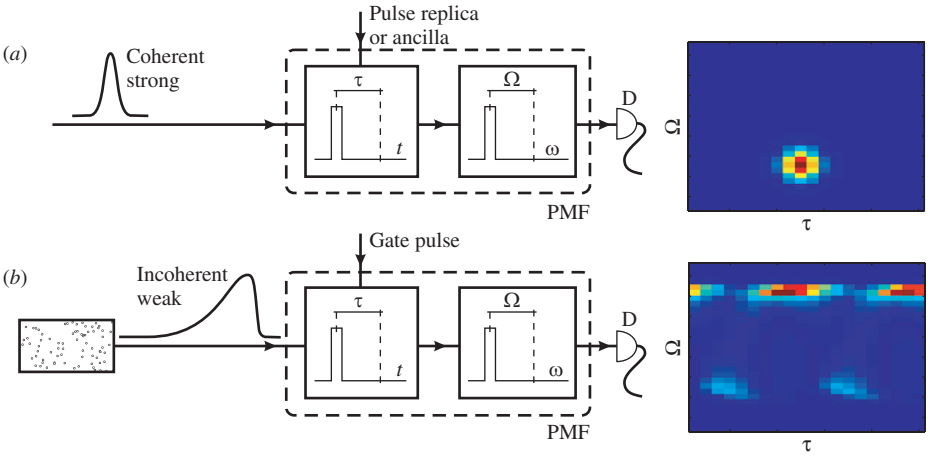

Figure 12. Analogy between (*a*) the spectrographic measurement of ultrashort laser pulse and (*b*) time-resolved emission spectroscopy of molecular fluorescence. In both cases the measured field if filtered through a time gate τ and a frequency gate Ω arranged in series and an integrating detector D is used afterwards. Both gates can be realized simultaneously by PMF of type I nonlinear crystal. (The colour version of this figure is included in the online version of the journal.)

From the tomographically complete measurements a representation of the quantum state in phase space can be reconstructed by means of the inverse Radon transform [30, 31]. Recently the Maximum Likelihood (ML) estimation of the quantum state has also been proposed [36]. In the latter one tries to find the state that is most likely to produce the measured data set and since *a priori* knowledge about the state is used, the statistical errors are significantly reduced, though at the expense of higher computational complexity. Because the ML state estimation problem has n^2 free variables for an n-dimensional Hilbert space, the number of different time and frequency settings also needs to be at least n^2 in order to be tomographically complete. The ML estimation of the process requires even more data, since the number of free variables is $n^4 - n^2$.

Quantum tomography experiment using spectral filtering properties of type I nonlinear crystal for simultaneous time and frequency gating of molecular fluorescence is shown in figure 13.

The vibrational wavepacket was excited in potassium dimers with 90 fs, 1 μJ resonant laser pulses at 840 nm. Sum frequency generation in a 3 mm thick, type I BBO crystal was used for both time- and frequency gating of the broadband molecular fluorescence at a level of less than one photon per spatio-temporal mode. The frequency window created by PMF for 3 mm BBO crystal has a width of about 2 nm, which is narrow enough to resolve the fluorescence for tomographic reconstruction. The central wavelength of the filtered up-converted signal is tuned by changing the crystal angle. The up-converted light was detected using a photo-multiplier tube in photon counting mode.

In figure 14 we show an example of the time- and frequency-resolved fluorescence as a function of time delay, for two different frequencies and

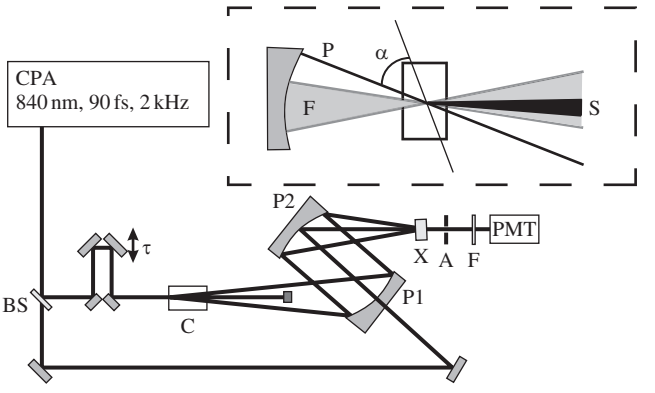

Figure 13. Experimental setup used for molecular emission state tomography. The fluorescence emitted from molecules in cell C is time gated by mixing with strong pump pulse in 3 mm BBO crystal X. The up-converted light is filtered spatially by aperture A and colour filter F and recorded by the photomultiplier PMT. The insert shows details of the crystal arrangement (in side view): P—pump beam, F—fluorescence beam, S—upconverted signal beam, α—crystal tuning angle defining the spectral gate position.

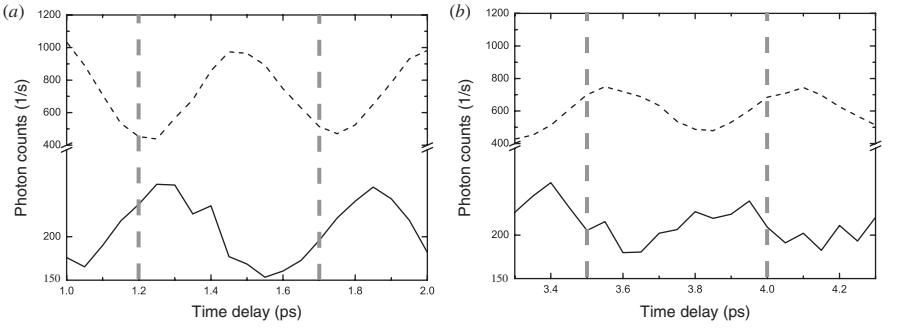

Figure 14. The fluorescence of (*a*) a well-localized and (*b*) de-localized wavepacket, at 1065 nm (dashed line) and 957 nm (solid line) measured in time delay steps of 50 fs. Dashed lines indicate one-period time windows used in process tomography.

two different wavepackets. The modulation of the signal corresponds to the 500 fs periodic motion of the wavepacket. At 1065 nm (dashed line) the wavepacket is at the outer turning point of the oscillatory motion, where it resides longest and thus emits more fluorescence. At 957 nm the wavepacket is almost at the inner turning point and the modulation of that signal is almost out of phase with the outer turning point signal. In figure 14(*a*) the signal corresponds to a localized wavepacket, while in figure 14(*b*) it corresponds to a de-localized wavepacket—the wavepacket localization is clearly reflected in the modulation depth. If the wavepacket is completely de-localized the Wigner distribution is spread out over the entire phase space

trajectory and the signal is constant in time; the signal depends only on the setting of the frequency gate.

As the broadband excitation generates a wavepacket which occupies around 6 vibrational levels, for state tomography at least 36 different settings are required, e.g. 6 delays within one oscillation period and 6 frequency settings. For process tomography as many as 1260 different settings would be required. The number of required settings is smaller when the different input states are taken into account and can be reduced further by employing more elaborate process tomography schemes.

6. Concluding remarks

Understanding the phase matching in birefringent nonlinear crystals has already provided new opportunities in a number of applications. Making use of the spectral properties of the interacting fields instead of resorting to additional filters allows for a simpler, more elegant and often more efficient implementation of experiments involving frequency conversion.

Although the examples described herewith may at first seem to be limited to a specific wavelength in combination with certain crystals, there have already been a few schemes proposed to extend the available spectral range. First, one can match not the group velocities of the interacting fields but rather their projections onto a certain axis in the noncollinear geometry—a scheme known from broadband second harmonic generation [37, 38] and parametric amplification of femtosecond laser pulses [39, 40].

Secondly, optical microstructures open a way towards manipulating dispersive properties of the composite materials [41, 42]. One such solution has been recently demonstrated, in which the layers of nonlinear birefringent crystal are interspersed with a linear material exhibiting inverse group delay [43]. The scheme was successfully used for generating photon pairs described by a joint spectral amplitude with arbitrary degree of entanglement. The method may be potentially implemented to obtain a broad range of states including factorable states as well as states engineered specifically for Hong–Ou–Mandel interferometry.

Acknowledgements

We are grateful for conversations with a number of colleagues on the issues discussed in this paper, including Christine Silberhorn, Michael Raymer, Czesław Radzewicz, Konrad Banaszek, and Wojciech Wasilewski. The work reported in this paper was completed under a number of different research projects. We acknowledge support by the EC under the Integrated Project QAP funded by the IST directorate as Contract No. 015848 (JL, IAW), by the ARO-QA program contract DAAD19-02-1-0163 (MB, IAW), by MNiSW under grant N202 019 32/0698 (PW), by Conacyt under grant 46370-F (AU), and by EPSRC under grants EP/D503248/1 (PW, IAW) and EP/C013840/1 (PM, JL, IAW) and by the Weiner-Anspach Foundation (SPG).

References

[1] J.A. Armstrong, N. Bloembergen, J. Ducuing, *et al.*, Phys. Rev. **127** 1918 (1962).
[2] J.A. Giordmaine, Phys. Rev. Lett. **8** 19 (1962).
[3] P.D. Maker, R.W. Terhune, M. Nisenoff, *et al.*, Rev. Lett. **8** 21 (1962).
[4] S. Somekh and A. Yariv, Opt. Commun. **6** 301 (1972).
[5] J. Comly and E. Garmire, Appl. Phys. Lett. **12** 7 (1968).
[6] W. Glenn, IEEE J. Quantum Electron. **5** 284 (1969).
[7] A.P. Baronavski, H.D. Ladouceur and J.K. Shaw, IEEE J. Quan. Electron. **29** 580 (1993).
[8] A.P. Baronavski, H.D. Ladouceur and J. K. Shaw, IEEE J. Quan. Electron. **29** 2928 (1993).
[9] K. Osvay and I.N. Ross, J. Opt. Soc. Am. **B** 13 1431 (1996).
[10] C. Radzewicz, P. Wasylczyk and J.S. Krasiñski, Opt. Commun. **186** 329 (2000).
[11] K.A. O'Donnell and A.B. U'Ren, Opt. Lett. **32** 817 (2007).
[12] D. Bouwmeester, J.-W. Pan, K. Mattle, *et al.*, Nature **390** 575 (1997).
[13] D. Boschi, S. Branca, F. De Martini, *et al.*, Phys. Rev. Lett. **80** 1121 (1998).
[14] J.W. Pan, D. Bouwmeester, H. Weinfurter, *et al.*, Phys. Rev. Lett. **80** 3891 (1998).
[15] E. Knill, R. LaFlamme and G.J. Milburn, Nature **409** 46 (2001).
[16] A.B. U'Ren, Y. Jeronimo-Moreno and H. Garcia-Gracia, Phys. Rev. A **75** 023810 (2007).
[17] W. Mauerer and C. Silberhorn, quant-ph/0609195 (2006).
[18] W. Wasilewski, A.I. Lvovsky, K. Banaszek, *et al.*, Phys. Rev. A **73** 063819 (2006)
[19] W.P. Grice, A.B. U'Ren and I.A. Walmsley, Phys. Rev. A **64** 063815 (2001).
[20] A.B. U'Ren, Ch. Silberhorn, R. Erdmann, *et al.*, Laser Phys. **15** 146 (2005).
[21] V. Wong and I.A. Walmsley, J. Opt. Soc. Am. B **12** 1491 (1995).
[22] C. Dorrer and I.A. Walmsley, EURASIP J. App. Sig. Proc. **10** 1541 (2005).
[23] C. Iaconis and I.A. Walmsley, IEEE J. Quan. Electron. **35** 501 (1999).
[24] A.S. Radunsky, S.P. Gorza, P. Wasylczyk, *et al.*, Opt. Lett. **32** 181 (2007).
[25] A.S. Radunsky, E.M. Kosik, I.A. Walmsley, *et al.*, Opt. Lett. **31** 1008 (2006).
[26] S.-P. Gorza, A.S. Radunsky, P. Wasylczyk, *et al.*, J. Opt. Soc. Am. B (accepted).
[27] I.A. Walmsley and V. Wong, J. Opt. Soc. Am. B **13** 2453 (1996)
[28] W. Wasilewski, P. Wasylczyk and C. Radzewicz, Appl. Phys. **B 78** 589 (2004).
[29] M.P.A. Branderhorst, P. Wasylczyk and I.A. Walmsley, Appl. Phys. Lett. **88** 061109 (2006).
[30] U. Fano, Rev. Mod. Phys. **29** 74 (1957).
[31] K. Vogel and H. Risken, Phys. Rev. A **50** 4298 (1989).
[32] I.L. Chuang and M.A. Nielsen, J. Mod. Opt **44** 2455 (1997).
[33] T. Dunn, J. Sweetser, I.A. Walmsley, *et al.*, Phys. Rev. Lett. **70** 3388 (1993).
[34] T. Dunn, I.A. Walmsley and S. Mukamel, Phys. Rev. A **74** 884 (1995).
[35] P. Kowalczyk, C. Radzewicz, J. Mostowski, *et al.*, Phys. Rev. A **42** 5622 (1990).
[36] K. Banaszek, G.M. D'Ariano, M.G.A. Paris, *et al.*, Phys. Rev. A **61** 010304 (1999).
[37] O.E. Martinez, IEEE J. Quan. Electron. **25** 2464 (1989).
[38] P. Baum, S. Lochbrunner and E. Riedle, Opt. Lett. **29** 1686 (2004).
[39] G.M. Gale, M. Cavallari, T.J. Driscoll, *et al.*, Opt. Lett. **20** 1562 (1995).
[40] A. Shirakawa and T. Kobayashi, Appl. Phys. Lett. **72** 147 (1998).
[41] J. Huang, J.R. Kurz, C. Langrock, *et al.*, Opt. Lett. **29** 2482 (2004).
[42] R. Lifshitz, A. Arie and A. Bahabad, Phys. Rev. Lett. **95** 133901 (2005).
[43] A.B. U'Ren, R.K. Erdmann, M. de la Cruz-Gutierrez, *et al.*, Phys. Rev. Lett. **97** 223602 (2006).